Surviving the Surf: The Tribomechanical Properties of the Periostracum of *Mytilus sp*

Felix C. Wählisch, Nicolas J. Peter, Oscar Torrents Abad, Mariana V. G. Oliveira, Andreas S. Schneider, Wolfgang Schmahl, Erika Griesshaber, and Roland Bennewitz

Keywords:
Periostracum, mytilus, friction, wear, nanoindentation

Formal publication in *Acta Biomaterialia*, http://dx.doi.org/10.1016/j.actbio.2014.05.014

Surviving the surf: The tribo-mechanical properties of the periostracum of *Mytilus* sp.

Felix C. Wählisch[1,2], Nicolas J. Peter[1], Oscar Torrents Abad[1], Mariana V.G. Oliveira[1], Andreas S. Schneider[1], Wolfgang Schmahl[3], Erika Griesshaber[3], Roland Bennewitz[1,2]

[1] INM-Leibniz Institute for New Materials, Campus D2 2, 66123 Saarbrücken, Germany

[2] Experimental Physics, Saarland University, Campus D2 2, 66123 Saarbrücken, Germany

[3] Ludwig Maximilian University of Munich, Theresienstrasse 41, 80333 Munich, Germany

Published in Acta Biomaterialia, 10 (2014) 3978–3985

Keywords: Periostracum, Mytilus, Friction, Wear, Nanoindentation

Abstract

We investigated the friction and wear behavior as well as the mechanical properties of the periostracum of *Mytilus* sp. Tribological properties were determined with a reciprocal sliding microtribometer, while mechanical characterization was done using a nanoindenter. Measurements were performed in dry and wet conditions. On the dry periostracum we found a low friction coefficient of 0.078+/-0.007 on the young parts and a higher one of 0.63+/-0.02 on the old parts of the shell. Under wet, saline, conditions we only observed one average coefficient of friction of 0.37+/-0.01. Microscopic *ex situ* analysis indicated that dry periostracum wore rather rapidly by plowing and fatigue, while it exhibited a high wear resistance when immersed in salt water. The Young's modulus and hardness of the periostracum were also investigated in both, dry and wet conditions. Under dry conditions the Young's modulus of the periostracum was 8+/-3 GPa, while under wet conditions it was 0.21+/-0.05 GPa, respectively. The hardness of dry periostracum samples was 353+/-127 MPa whereas of wet samples it was 5+/-2 MPa. It was found that, in wet state, viscous behavior plays a significant role in the mechanical response of the periostracum. Our results strongly indicate that the periostracum can provide an important contribution to the *Mytilus* sp. shell's overall wear resistance.

1 Introduction

The common blue mussel of the genus *Mytilus* is highly adaptable to distinct habitats. It inhabits freshwater [1, 2, 3] as well as brackish [4] and marine environments ranging from the shallow temperate to boreal waters [5]. The shells of species within the genus of *Mytilus* are composed of three layers: the outer, organic periostracum and the two inner, calcified layers. The periostracum, the outmost organic layer is a quinone-tanned sclerotinized protein cap [6] that covers the exterior of the shell of almost all mollusks [7]. It has a variable thickness and microstructure, such that in some bivalve species it is very prominent while in others it is hardly visible [7]. While scientific aspects of the calcareous part of bivalve shells have been investigated extensively (e.g. [8, 9, 10, 11, 12, 13]) little attention was given to the periostracum. The periostracum is an integral part of the shell and serves several, distinct and major roles. It not only protects the carbonate hard tissue against environmental stress and dissolution, it also seals extrapallial space where supersaturation conditions

required for shell mineralization have to be maintained [14]. The periostracum consists of distinct layers that serve as templates for carbonate crystal nucleation and thus shell formation [6, 7, 15, 16, 17, 18, 19, 20].

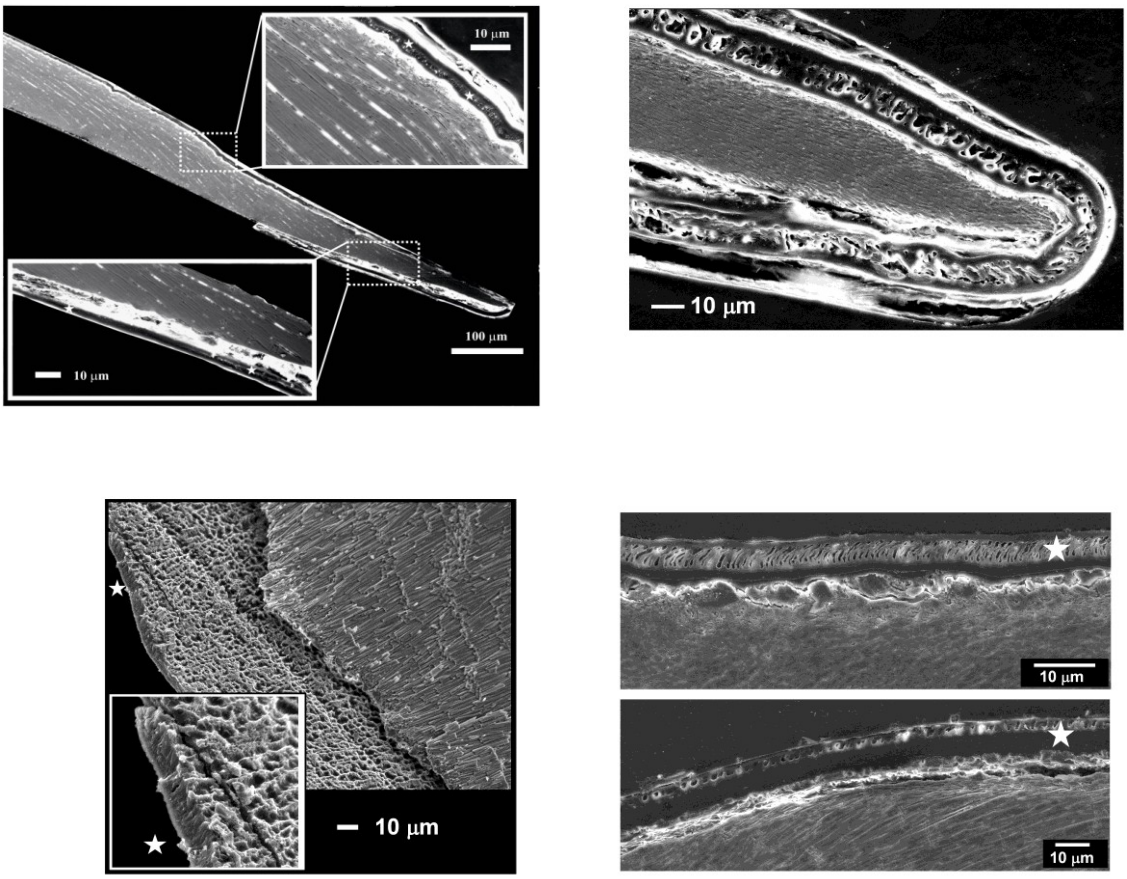

Fig. 1: *SEM images of the periostracum and the fibrous calcitic shell layers of Mytilus edulis. Well visible in (a) and (b) is the encasement of the hard tissue by the periostracum. Within the inserts of (a) stars mark the location of the periostracum at the seaward (upper insert) and at the innermost shell portion (lower insert). (c) Interface between the periostracum and the stacks of calcite fibers. Figures 1b and 1d show the prominent vacuolized central periostracum layer.*

In a developing mollusc embryo and at shell repair [21, 22] the periostracum is the first-formed tissue. It develops in the periostracal groove that is located between the outer and middle folds of the mantle tissue [17, 18, 19, 20, 23, 24]. At the start of secretion it is formed by cells that border the shell gland [7]. At a later developmental stage, it is formed by the mantle tissue. In the course of its movement from the periostracal groove the periostracum thickens and, at a certain stage, spans from the edge of the mantle lobe to the extreme edge of the valve [7, 19]. At this position it is not influenced by mantle cells any more. It is differentiated into distinct layers and does not increase in thickness. On its inner surface, it is in contact with extrapallial fluid, while its outer surface is in touch with sea water. Just beyond the edge of the carbonate shell the periostracum doubles back on itself [7, 19] (Figure 1a) and covers the outside of the mantle lobe and the secreted shell. Checa [19] showed for Unionidae that at the shell margin the middle layer of the periostracum becomes vacuolized. These cavities get filled with aragonite and eventually form (in the case of Unionidae) the outer prismatic shell layer. At the inner periostracum sheet the nacreous layer of the shell is formed [19].

Kessel [25, 26], Dunachie [21], Bubel [22] as well as Waite and Anderson [27] investigated in great detail periostracum formation, development and repair of Mytiloidae. This genus has a thick, tri-

layered periostracum with the central periostracum layer being often vacuolated (Figure 1b). Mytiloidae need a thick and protective periostracum since their habitat is mainly the intertidal region. They are exposed to harsh and highly varying environments that range from direct insolation at low tide to high energy surges at high tide.

Resistance to impact and fracture of the calcified shell has been well studied for bivalves and gastropods, however, friction behavior and wear resistance is only little investigated. Even though external forces hit first the periostracum, studies dealing with friction and wear of mollusk shells investigate the carbonate shell portions only and disregard the periostracum [28]. Often, macroscopic tribometers like a block-on-ring tribometer [29] are used, where, by omitting the initial phase of running-in, the role of the periostracum is not considered. In an initial experiment concerning the wear behavior of the periostracum Tong *et al*. [30] performed an experiment where bivalve shells were pressed through sand. The wear rate was measured by means of weight loss. Abrasive wear was found to be higher when the sliding direction was parallel to the valve corrugation. It was also increased for larger abrasive particles and higher sliding velocities. All experiments known to us were performed only in dry conditions, and, thus, do not reflect natural living conditions.

Mytilus sp. lives in shallow waters, thus in a surf environment. The shell is permanently exposed to friction by contact to differently sized sand particles and pebbles that are driven by wave motion. Thus, protection against periostracum abrasion is of major and lifelong importance to the animal. The major aim of our study is to investigate the contribution of the periostracum of *Mytilus* sp. to the shell's overall friction and wear resistance. *Mytilus* sp. were chosen due to their highly varying and partly extreme habitat conditions. For a profound understanding we conducted all experiments in both, dry and wet states. In order to resolve the mechanical and structural contributions of the different layers of the periostracum, we applied a multi-analytical approach, focusing on measurements with a very high spatial resolution.

2 Materials and methods

Live bivalve specimens of *M. galloprovincialis* and *M. edulis* were obtained and investigated. As no mechanical differences were found, we refer to them as *Mytilus* sp. The valves were opened, cleaned with tap water, and stored dry under laboratory conditions. The valves of ten different animals were tested. Tribological tests were performed on seven animals while nanoindentation measurements were done on three *Mytilus sp.* samples. Since friction measurements reveal local variations of mechanical properties of the periostracum larger than variation between different valves, the detailed investigation of one bivalve specimen was considered to be appropriate.

For SEM imaging the shells were sectioned along their median plane and about 1 mm thick shell wafers were cut out. The wafers were embedded into a cold mounting epoxy-based resin and were treated with eight sequential mechanical polishing steps down to a grain size of 1 μm. For the final step, etch-polishing with colloidal silica (particle size ~ 0.06 μm) in a vibratory polisher was applied.

For friction, wear resistance and nanoindentation measurements, one valve was glued onto a petrographic glass slide with UHU Repair All Powerkit (UHU GmbH & Co KG, Germany) such that the flattest part of the shell, the plane part at the commissure was roughly parallel to the plane of the glass slide.

Artificial sea water was used for the generation of wet conditions and was produced using 37.00 g Tropic Marin® sea salt (Dr. Bienet GmbH, Germany) and 950 ml MilliQ water. The pH was adjusted to 8.0 - 8.2 and the density to 1.022 kg/l – 1.024 kg/l. Evaporation was quantified using an Osmomat 030 (Gonotec, Germany) and found to be insignificant over the duration of one set of measurements.

The linear reciprocal sliding experiments were carried out using a home-built microtribometer. It consists of a dual double leaf spring with a normal stiffness of 2809 N/m and a lateral stiffness of 3722 N/m, whose deflections in both directions were measured by means of fiber optical sensors as described in [31, 32]. The counter body, also referred to as probe, was a 500 μm diameter stainless steel sphere, glued with H21D (Epoxy Technologies Inc., USA) to a M 1.6 stainless steel screw, where the extension of the threaded rod allowed for measurements in water without immersing the whole tribometer. For each experiment, a flat part of the shell was approached to the counter body to a pre-

set normal load. For the measurement, the shell was moved in a reciprocal manner for at least 512 cycles with a linear speed of 1 mm/s over a distance of 1 mm. The motor position and the signals of the fiber optical sensors are recorded at 512 (or more) time equidistant points along each half cycle. Data evaluation procedures are described in [33]. Essentially, friction was evaluated as average of full cycles of forward and backward probe movement, thereby minimizing effects of topography on friction signals. In figure 2(a) the microtribometer in the filled water tub is shown. Furthermore, the commissure of the shell can be seen. We refer to areas towards the center of the shell as the older shell portion and areas close to the rim (the commissure) as the young parts of the shell, as depicted in figure 2(b). We performed standard and long term friction experiments in wet and dry conditions. All experiments were conducted under laboratory conditions, being 21°C +/1°C.

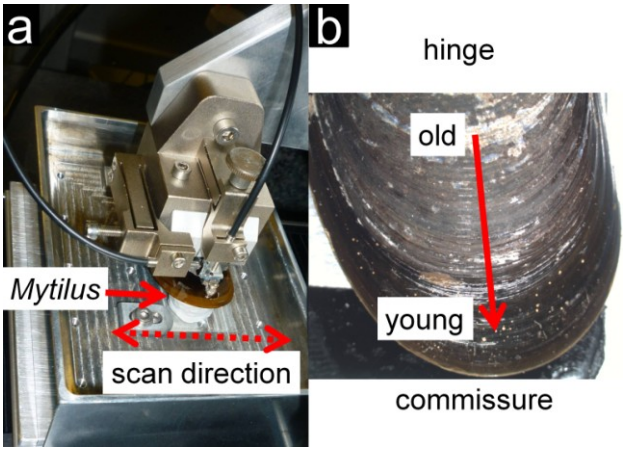

Fig. 2: *The microtribometer measurement setup. (a) the mollusk is immersed in sea water that is covered with parafilm that prevents evaporation. The parafilm is removed for the presented image. (b) Mytilus sp. valve depicting the commissure and the hinge of the shell and highlighting regions that are of interest for this study.*

Both, the young and the older parts of the shell were investigated. In standard experiments we conducted 512 friction cycles, while long term experiments lasted for several thousand cycles. The longest experiment with 16000 cycles was performed in wet condition and lasted for about 9 h (see Figure S1c). We designed three types of experiments: (a) in entirely dry condition, (b) in wet condition, where the sample was immersed in salt water prior to the start of the first cycle, and (c) experiments where the periostracum was wetted while the cycles were taken, thus, the experiment started in dry condition and finished in the wet state. The conditions used in the tests were a first order estimate of natural habitat conditions of *Mytilus sp*. In addition, care was taken to apply analytical conditions to factors that were significant to the investigated mechanical properties.

Load-controlled nanoindentation experiments were performed with a Triboindenter TI 950 (Hysitron Inc., USA) using a standard diamond Berkovich probe. For dry measurements, each measurement consisted of a 10 s loading, 10 s holding and a 10 s unloading part. On each position three maximum loads (0.5 mN, 5.0 mN and 13.0 mN) were tested consecutively in the same spot. To adapt to the viscous creep behavior of the periostracum in water, the measurement procedure was changed. After a 10 s loading to 2 mN, the load was kept constant for 60 s in order to omit most of the creep during the initial unloading within 10 s. Data were evaluated using Hysitron software, according to the well-established method of Oliver and Pharr [34]. Dry indents were implemented along a line from the older part of the shell up to the commissure; wet indents were performed in a millimeter-sized 10x10 matrix on an old part of the shell. Dry indents caused plastic deformation.

Modulus maps were taken over a cross-section of the wet and dry periostracum, also using the Triboindenter TI950 equipped with a dynamic force transducer (nanoDMAIII)), and either a standard or a fluid cell Berkovich tip depending on the measurements conditions; i. e. dry or wet, as described above. In order to acquire a modulus map, the indenter tip is raster-scanned over the surface of the sample in a similar manner to an atomic force microscope. In our experiments we applied a constant

contact force of 6 µN and recorded a surface topography map. Simultaneously, the local elastic modulus was measured by adding a small sinusoidal modulation force with an amplitude of 0.2 µN and a frequency of 220 Hz to the constant force. The amplitude of the modulated displacement is in the range of one nanometer in both measurements conditions. The material response causes a phase lag between modulation force and the resulting modulated indenter displacement. From the phase lag, displacement amplitude, frequency, and the tip area function, the storage modulus *E´* and the loss modulus *E´´* [35, 36] can be determined. In order to emphasize their physical meaning we will refer to storage modulus as stiffness and to loss modulus as viscosity synonymously within this paper.

SEM imaging was performed on fractured and highly polished surfaces. For this purpose 300 µm thick wafers were cut out along the longest axis of the shell from the hinge to the commissure. The wafers were embedded and were treated with several mechanical polishing steps. For the final step, chemical mechanical polishing with colloidal silica in a vibratory polisher was applied. The samples were coated with 15-20 nm of carbon. Images were obtained at 20 kV on an FEG-SEM (JEOL JSM 6400).

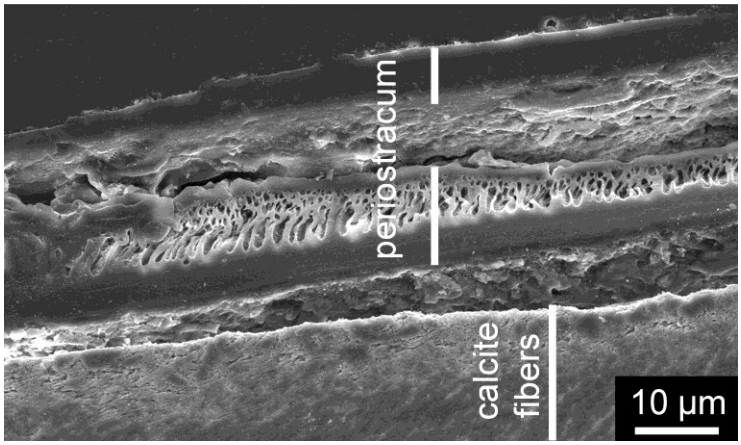

Fig.3: *SEM image of the periostracum plating the calcite fibers of the shell. Well visible is the layered nature of the periostracum, the dominant central vacuolized part that is bordered by two dense layers.*

3 Results

3.1 Periostracum structure and microstructure

Figures 1, 3 and 4 highlight for *Mytilus edulis* the microstructure of the periostracum that covers the carbonate hard tissue from the commissure to the hinge. Its thickness along the exterior of the carbonate shell is quite uniform and varies in the specimen shown in Figure 1d between 8 to 9 micrometers. As it is well visible in Figure 1c, there is a thin interface layer between the periostracum and the calcite fibers of the carbonate mineral tissue. The periostracum of *Mytilus sp.* is structured and consists of three layers. The central layer is highly vacuolized (Figures 1b, 1d, 3, 4) in general consisting of parallel, elongated vacuoles (Figures 3 and 4). However, as it is observable in the lower image of Figure 1d, the vacuolized layer can also exhibit a slightly different fabric. The vacuoles can also be round shaped and might accumulate along the seaward pointing part of the periostracum (lower image of Figure 1b). Vacuolization of the periostracum increases as the hinge is approached (Figure 3). The band of vacuoles is not as continuous at the hinge as it is at the tip of the valve (Figures 3 and 4). It is interrupted at regular intervals of 60-70 micrometers by 10-20 micrometers wide solid inlays (Figure 4). SEM imaging was done with both, an environmental as well as a high-resolution FEG-SEM. In both cases we observed the prominent vacuolized layer within the periostracum of *Mytilus sp.* In our opinion the vacuoles are not created by shrinkage of the periostracum due to dehydration. If this were the case, the vacuoles would be randomly distributed within the periostracum and would not be limited to its central portion.

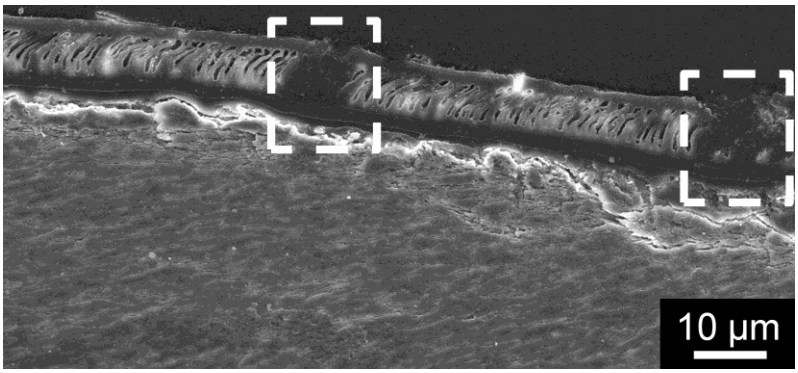

Fig. 4: *SEM image of the periostracum close to the hinge of the shell. In these shell segments the vacuolized layer is interrupted by more or less equidistant solid sections (inlays), highlighted in the image by white squares.*

3.2 Friction and wear in dry and wet conditions

Figures 5, S1, and S3 show friction data obtained for dry and wet conditions on young and old parts of the periostracum of *Mytilus* sp. In dry conditions we detected two distinct friction states for the periostracum (Figure 5a, b): a low friction state with a remarkably low coefficient of $\mu = 0.078 \pm 0.007$ measured only on the young parts of the shell and a high friction state with a significantly higher coefficient of $\mu = 0.63 \pm 0.02$ detected on both, the young and the older parts of the shell. The data in Fig. 5b represent 25 experiments for the low friction state and 70 experiments for the high friction state, recorded at varying load. Friction coefficients were determined by least-square linear fits to the data, following Amontons' law $F_L = \mu F_N$.

The coefficient of friction of the calcite fibers below the periostracum was $\mu = 0.81 \pm 0.02$ in dry conditions (see Figure 5a). This coefficient was determined from three friction experiments at equal load on a patch where the periostracum was chemically removed with perchloric acid; exemplary results are shown for both dry and wet state in Figure S1. A typical evolution of the local coefficient of friction from young (low friction) to old parts (high friction) of the shell in dry state is presented in Figure S3. The left part of the image shows the commissure of the shell with the positions of the experiments highlighted. On the right part, the corresponding coefficient of friction is plotted. During standard experiments (512 cycles) the periostracum always withstood the tribological load while it usually failed during long term experiments conducted on dry shells. This is highlighted by Figure S2a, which shows wear tracks after long experiments under dry conditions. Wear particles are visible along the wear track and at the turning points. Measurements on the calcite fibers of an etched shell where the periostracum was removed with acid also produced wear particles (Figure S1b).

On wet shells even in very long term experiments that lasted for several thousand cycles the periostracum was **never** destroyed entirely: Thus, the calcite fibers were never reached. Periostracum wear behavior in dry conditions on the other hand varied between an occasional early failure and fatigue failure which is shown in Figure S1. All long term experiments as well as some standard experiments in dry state that initially exhibited the low friction state with a friction coefficient around 0.078 featured a transition to the higher friction state with friction coefficients around 0.63.

When water was added to an initially dry experiment a rapid change within 10 cycles in the coefficient of friction occurred. Unlike in dry state, an average coefficient of friction of $\mu = 0.37 \pm 0.01$ was found (Figure 5c and d, determined from 74 experiments) irrespective of the position on the shell. Lateral force fluctuations were larger in wet than in dry experiments, as observed when comparing Figure 5a and c.

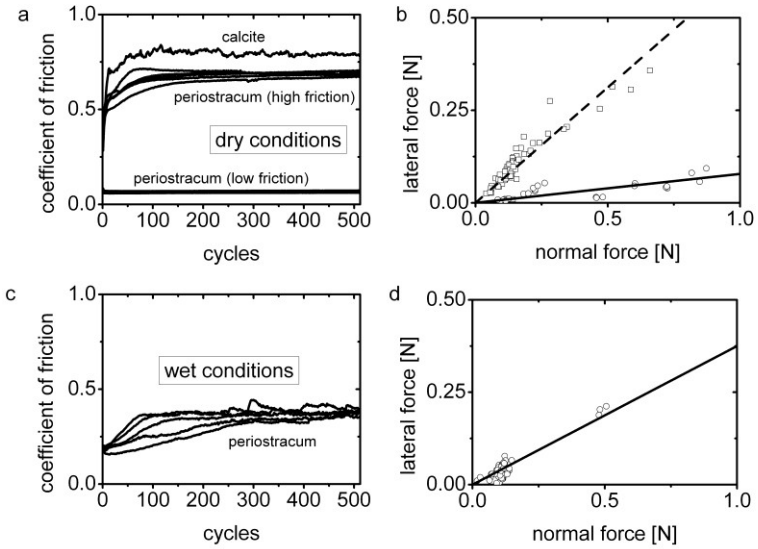

Fig. 5: *Results of tribological experiments. (a) Example curves for the coefficient of friction as function of time (cycle number) recorded in dry conditions. On the periostracum, either a low friction state (lowest set of curves) is found on younger parts or a high friction state (middle set of curves) is found predominantly on older parts, see text for details. On calcite fibers, exposed by etching of the periostracum, the highest friction is found (uppermost curve). (b) Evaluation of the friction coefficients from sets of experiments in dry conditions (circles low friction state, squares high friction state). Lateral force values are the average of the last 20 cycles of each experiment. (c) Example curves for the coefficient of friction as function of time (cycle number) recorded in wet conditions on the periostracum, found to be independent of position on the shell. (d) Evaluation of the friction coefficient from sets of experiments for wet conditions on the periostracum.*

Microtribological measurements conducted in wet conditions were followed by careful inspection in a light microscope. We did not find any wear scars on the wet periostracum surfaces by light microscopy, even after a measurement with 16000 friction cycles. A profilometric analysis of the tested area revealed a dimple of only 10 µm depth (see supplementary Figure S2b).

Wet state measurements performed directly on the fibrous layer below the periostracum showed a similar coefficient of friction value as obtained on the wet periostracum, i.e. of the order of $\mu = 0.4$. However, in contrast to the wet periostracum, we observed wear scars in the wet fibrous layer and corrosive wear of the counter body, indicated by flattening and rust formation at the sphere. In all experiments conducted on the wet periostracum we did not observe any corrosion or wear of the counter body. Instead, some material was transferred to the sliding sphere in both wet and dry friction experiments. Comparative measurements exhibited no friction difference between cleaned counter bodies and those with transferred material. Thus, we assumed that the transferred material has only a minor effect on the frictional response.

3.3 The Young's modulus and hardness of the periostracum in dry and wet conditions

Mechanical properties were determined for both, the dry and the wet periostracum states. In the dry condition, indentation scans started in the old shell portions and ended at the commissure, thus within young shell regions. Nanoindentation testing of the periostracum in wet condition was only performed in one region, as friction was observed not to differ between different regions on the wet periostracum. Typical force-displacement and displacement-time curves are presented in supplementary Figure S4. The indents performed on the dry periostracum exhibit no changes in stiffness with indentation depth, nor do they feature significant creep like for a polymer, the deformation is mostly plastic. The measurements on wet samples on the other hand, are dominated by viscous creep and the material is much less stiff. In order to evaluate Young's modulus, we discarded all measurements which did not

reach the load setpoint or creeped out of the displacement range of the force transducer. All remaining measurements had an identical stress history, allowing for determination of comparable values.

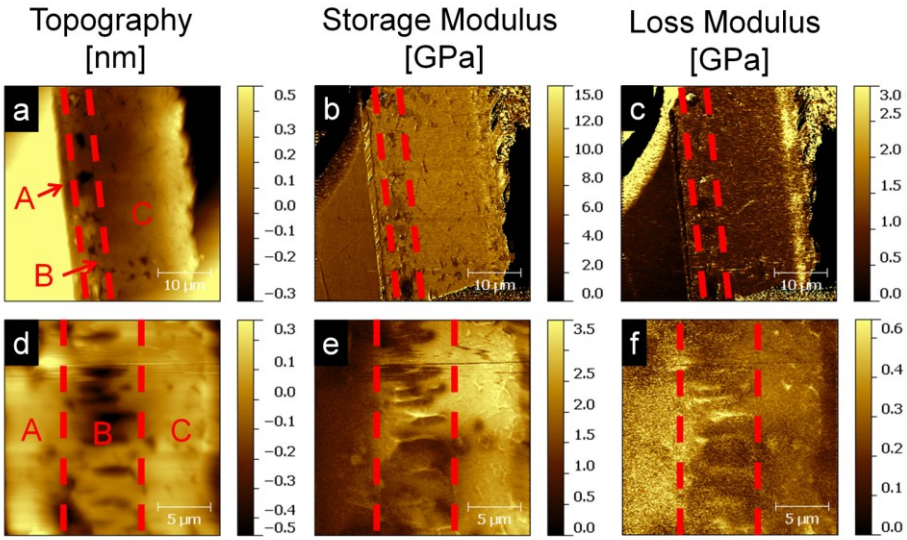

Fig. 6: *Topography and modulus maps for Mytilus sp. determined in dry (a), (b), (c) and in wet (c), (d), (e) conditions. A denotes the seaward pointing part of the periostracum, while C is its part next to the calcite fibers. The images do not show modulus mapping results of the calcite fibers. A distinct change in viscoelastic properties can be seen when the areas A and C are compared to each other.*

The mean Young's modulus of the dry periostracum is (8 ± 3) GPa while for the wet periostracum it is only (0.21 ± 0.05) GPa. The mean hardness of the dry periostracum is (353 ± 127) MPa, while for the wet periostracum it is as low as (5 ± 2) MPa. Considering the significant natural corrugation of the shell's surface there is little scatter in the material properties data. A difference between old and young shell portions under dry conditions is found neither for the hardness nor for Young's modulus, in contrast to the tribological tests.

3.4 Modulus mapping in dry and wet condition

The periostracum of *Mytilus* sp. is structured and is composed of at least three layers. In order to gain a deeper understanding about the protective function of the periostracum, the mechanical properties of each of these three layers had to be resolved. This was done by modulus mapping experiments performed on a cross-section of the periostracum in wet and dry conditions. Modulus mapping requires flat sample surfaces that were achieved by polishing with a root-mean-square roughness of 40 nm for the periostracum layer between the vacuoles and the underlying calcite fibers (Figure 6, area C) and a root-mean-square roughness of 74 nm for the outermost, the seaward pointing periostracum layer (area A).

On the basis of the height image (Figure 6a) one can only distinguish between the central, highly vacuolized (area B) and the solid, bordering layers (areas A, C). However, the storage- (Figure 6b) and the loss-modulus (Figure 6c) images illustrate the difference between the seaward and the innermost periostracum layers. All three images highlight the presence of the vacuolized band within the central part of the periostracum (area B). Furthermore, a network of topographic trenches is highlighted in the modulus map. However, topographic features with dimensions comparable to the tip size are known to always produce a contrast in modulus maps. This effect is due to a local change in the contact area between tip and surface, which is an important parameter for the measured phase lag. Therefore, modulus contrast at steep topographic features is mostly a measurement artifact rather than a real change in modulus. Vacuole depths were in the range of several hundred nanometers, even though precise depths were difficult to determine, as the pyramidal indenter tip often did not reach the very bottom of each cavity. A further topographic feature, a depression, is well visible at the very right end

of topography image. It corresponds to a crack present between the fibrous calcite layer and the periostracum which has most probably been introduced during preparation.

Starting with a low storage modulus of about 0.5 GPa at the seawards pointing area A, it increases to a higher modulus of about 1.75 GPa at the inner part close to the calcitic fibers, area C. The loss modulus also exhibits a contrast between outer and inner part of the periostracum, a higher loss modulus of about 0.25 GPa is measured at the outer (area A) and a lower of about 0.15 GPa at its inner part (area C) next to the fibrous calcite layer. Thus, the storage and loss modulus maps reveal a significant variation of mechanical properties across the cross-section of the periostracum, such that the innermost periostracum layer, the layer next to the calcite fibers (area C) is the most elastic portion, while the seaward pointing part of the periostracum (area A) is significantly less elastic but more viscous. We attribute these observations to a different swelling behavior of layer A and C, which consequently cannot be observed in dry state. An artifact due to a local contamination of the layer can be excluded, because the chemical composition of the periostracum does not vary significantly and no variation of possible contamination across the periostracum is expected.

4 Discussion

4.1 Structural characteristics of a layered periostracum

In *Mytilus* sp. a thick organic periostracum forms the cover of the mineralized part of the shell. The interlinked entity of these two materials, the organic periostracum and the underlying mineralized hard tissue, yield the desired protection of the soft tissue of the animal. The periostracum is a unique material and is of profound importance. It not only plays an integral role in shell mineralization but it also protects the shell from (a) dissolution in acidic environments, (b) shell damage caused by harsh habitats and (c) shell destruction induced by predators. Because our intent was to understand the role of the periostracum in the protection of the hard carbonate and the soft tissue parts of the shell, we did not investigate its role in shell mineralization.

The complete coverage of the shell from the commissure to the hinge by the periostracum of uniform thickness and structure indicates its well defined function in shell protection. In addition, nanoindentation testing performed on the seaward pointing surface of the periostracum also shows its uniformity and thus protective nature, since there seem to be no major differences in hardness and Young's modulus between differently aged shell portions.

However, the examination of the cross-section of the periostracum reveals its highly structured nature not only concerning its ultrastructure but also its mechanical properties. The periostracum of *Mytilus* sp. is laminated and is composed of an extended vacuolized central layer that is bordered by two dense layers. While SEM imaging did not resolve any difference between the two dense layers, modulus mapping enabled us to demonstrate gradients in stiffness and viscosity across the cross-section of the periostracum. We also detected that these two properties have a reverse effect. Thus, taking the periostracum and the underlying calcite fibrous shell layer together we find a highly structured shell entity. Protection is ensured by the interplay of several specific material property characteristics such as elasticity (area A), combined with damping capabilities (area B), viscosity (area C) and hardness provided by the uppermost stacks of calcite fibres of the mineralized shell.

4.2 Advantages of a layered periostracum and its protective nature

On the **dry periostracum**, friction in most measurements either evolves from low to high values, or is high from the very beginning of the measurement. We consider the low friction state as a precursor of the high friction state. As the low friction state is found almost exclusively on the young parts of the shell, we assume that, at this portion of the shell, friction is reduced by a thin coating [21]. As we never observe the low friction state on older shell portions we assume that this thin coating wears off with time. However, as nanoindentation results show, the thin coating does not influence the hardness or the Young's modulus of the shell. Other possible explanations, like a sub-surface delamination process or plastic deformation of the underlying calcitic fibers might be considered. However, it should be noted that as long as the low friction state is maintained, almost no wear track is observed

on the surface of the sample. Once high friction conditions are reached, a distinct track is formed by either fatigue and plowing until the periostracum is destroyed.

In **wet conditions**, the coefficient of friction is neither particularly low nor high, but it stays constant under prolonged testing. Due to the low sliding speed we can disregard lubrication in the hydrodynamic regime. We assign the change in friction to changes not only in the interfacial interactions, but also to changes in viscoelastic response to the sliding tip, taking into account the nanoindentation results.

In contrast to the dry state, **the wear resistance in wet conditions is excellent**. We have clear indications that, even under prolonged testing, the periostracum remains intact: no wear tracks have been found by light microscopy after wet experiments, and no signs of corrosive wear at the counter body are observed, which are readily present when the calcitic fiber layer has been tested directly in wet condition. Nanoindentation experiments carried out in wet conditions reveal a highly viscous behavior of the periostracum. However, even though quantitative viscoelastic material properties are rather challenging to extract from indentation measurements [37, 38], their contribution towards wear resistance can easily be understood in a qualitative manner. A viscoelastic material behaves load rate dependent, such that it is hard when a sudden change in load (impact) is applied and behaves soft if the change is slow. Thus, the contact area during the sliding experiment will change with the velocity of the probe. Experiments and simulations for open pored hydrogels have demonstrated these features [39], and *Mytilus* sp. might show a similar behavior utilizing the vacuoles in the periostracum as a water reservoir that, on demand, might be squeezed out. Thus, prior to plastic deformation of the entire periostracum, the role of the vacuoles is that of a damper, being useful for contacts that are comparable in size to the thickness of the periostracum. Smaller contacts, however, interact with the outmost layer of the periostracum as demonstrated by nanoindentation. With its reduced Young's modulus in water, the periostracum cannot be considered a classical hard anti-scratch coating. Instead, the periostracum's wear resistance probably originates in viscous effects. As these only come into operation when immersed in water, the wear resistance is only present when actually needed.

4.3 Experimental tribology and the biological system

The major habitat of Mytiloidae is the intertidal region, a high energy marine environment where all sorts of differently shaped particles impact and abrade the shell. The counter body that we used in our experiments is a sphere made of steel, different in material and shape from sand grains. The arbitrary shape of 'natural' counter bodies hampers analysis based on contact mechanics. 'Laboratory' counter bodies on the other hand, enable meaningful evaluations as they are well defined and furthermore allow for comparison between experiments. As the observed material transfer to the sphere had no influence on the results, we believe that the material of the counter body plays a minor role in these experiments. In addition, corrosive wear of the steel sphere in contact with the calcitic fibers was discovered to be an excellent indicator for the complete wear off of the periostracum (see Figure S1).

In nature the shells are exposed to abrasive particles in breaking waves and the question arises whether sliding friction is the appropriate friction process that models natural conditions. The low Young's modulus actually favors rolling friction over sliding friction [40]. Microtribological rolling friction experiments on rough surfaces are experimentally challenging and have not yet been implemented by anyone, yet. Abrasion of the shell using a water jet with sand would mimic the natural conditions but would not allow for examinations normal and lateral forces. Considering that sliding friction usually leads to more severe wear than rolling friction, our experiments emphasize the remarkable wear resistance of the periostracum.

The mechanical properties of the periostracum derived from modulus mapping on its cross-section show a gradual increase of the storage modulus from outer (seaward pointing) to the inner part of the periostracum and a step-like decrease of the loss modulus from the layer above into the vacuolized periostracum region. In general, the periostracum's material is more compliant and viscous on the outside and rather stiff and more elastic on its inner parts next to the calcite fibers. At present, we do not know the mechanisms or the microstructures that create the gradient in storage modulus and we can also only speculate on the role of the vacuoles in the step-wise increase of loss modulus across the periostracum. We observe that the material is not fully homogeneous and the possible advantages of a

softer, viscoelastic surface in the defense against mechanical impact from the mollusk's environment should be addressed on future studies.

5 Conclusions

The main goal of this study is to investigate mechanical properties of the periostracum of *Mytilus* sp. in order to understand its protective nature for the hard and soft tissues of the animal. This has been done in a multi-analytical approach utilizing tribology and nanoindentation testing.

1. This is the first study that presents friction and wear experiments together with Young's modulus and hardness results of the periostracum of the modern bivalve *Mytilus* sp.
2. Nanoindentation testing carried out on the shell's outer surface does not show a difference in Young's modulus and hardness between differently aged shell portions. SEM imaging of the cross-section of the periostracum documents its even thickness from the commissure to the hinge. It also highlights its layered nature consisting of a highly vacuolized central and two bordering dense layers. The vacuolized layer in the periostracum of *Mytilus* sp. is highly prominent and forms a major part of the periostracum.
3. In dry condition a low and a high friction state were observed, while in wet condition only one intermediate coefficient of friction was measured. Wear resistance is low in dry condition, while it is high in wet condition. Even under prolonged testing in wet condition the periostracum remains intact and can hardly be destroyed.
4. Storage und loss modulus results resolve further the different layers and the structured nature of the periostracum. Viscosity and stiffness is graded across its cross-section such that an increased viscosity is coupled to a decreased stiffness and vice versa.
5. Taking all material property results together we can posit that the outermost dense periostracum layer is capable of repelling small impact events. In the case of prolonged or large impact events the outer dense and inner vacuolized layers interact and behave as one unit. In addition to the viscous behavior of the outermost dense periostracum layer the vacuolized layer behaves as a damper. This ensures that the effect of large impacts is averted and that little shell material is destroyed.

6 Acknowledgements

We thank Bentejuí Medina Clavijo for support when performing modulus maps and Eduard Arzt for continuous support of the project. E. Griesshaber and W. W. Schmahl thank the DFG for financial support.

Literature

[1] Shumway SE. Effect of salinity fluctuation on the osmotic pressure and Na+, Ca2+ and Mg2+ ion concentrations in the hemolymph of bivalve molluscs. *Marine Biology* 41(2):153–177, 1977.

[2] Gillikin DP, Dehairs F, Lorrain A, Steenmans D, Baeyens W, André L. Barium uptake into the shells of the common mussel (Mytilus edulis) and the potential for estuarine paleo-chemistry reconstruction. *Geochimica et Cosmochimica Acta*, 70(2):395–407, January 2006.

[3] Gillikin DP, Lorrain A, Bouillon S, Willenz P, Dehairs F. Stable carbon isotopic composition of Mytilus edulis shells: relation to metabolism, salinity,$\delta^{13}C_{DIC}$ and phytoplankton. *Organic Geochemistry*, 37(10):1371–1382, October 2006.

[4] Hietanen B, Sunila I, Kristoffersson R. Toxic effects of zinc on the common mussel Mytilus edulis L. (Bivalvia) in brackish water. 1. Physiological and Histopathological studies. *Annales Zoologici Fennici*, 25(4):341–347, 1988.

[5] Beesley A, Lowe DM, Pascoe CK, Widdicombe S. Effects of CO2-induced seawater acidification on the health of Mytilus edulis. *Climate Research*, 37(2-3):215–225, October 2008.

[6] Taylor JD, Kennedy WJ. The influence of the periostracum on the shell structure of bivalve molluscs. *Calcified Tissue Research*, 3(1):274–283, 1969.

[7] Harper EM. The molluscan periostracum: an important constraint in bivalve evolution. *Palaeontology*, 40(1):71–97, 1991.

[8] Addadi L, Joester D, Nudelman F, Weiner S. Mollusk Shell Formation: A Source of New Concepts for Understanding Biomineralization Processes. *Chem. Eur. J.*, 12(4):980–987, January 2006.
[9] Nudelman F, Gotliv BA, Addadi L, Weiner S. Mollusk shell formation: Mapping the distribution of organic matrix components underlying a single aragonitic tablet in nacre. *Journal of Structural Biology*, 153(2):176–187, February 2006.
[10] Jacob DE, Soldati AL, Wirth R, Huth J, Wehrmeister U, Hofmeister W. Nanostructure, composition and mechanisms of bivalve shell growth. *Geochimica et Cosmochimica Acta*, 72(22):5401–5415, November 2008.
[11] Hahn S, Rodolfo-Metalpa R, Griesshaber E, Schmahl WW, Buhl D, Hall-Spencer JM, Baggini C, Fehr KT, Immenhauser A. Marine bivalve geochemistry and shell ultrastructure from modern low pH environments: environmental effect versus experimental bias. *Biogeosciences Discussions*, 8(5):10351–10388, October 2011.
[12] Marin F, Roy NL, Marie B. The formation and mineralization of mollusk shell. *Frontiers in Bioscience*, S4:1099–1125, January 2012.
[13] Griesshaber E, Schmahl WW, Ubhi HS, Huber J, Nindiyasari F, Maier B, Ziegler A. Homoepitaxial meso- and microscale crystal co-orientation and organic matrix network structure in Mytilus edulis nacre and calcite. *Acta Biomaterialia*, 9(12):9492–9502, December 2013.
[14] Marin F, Luquet G. Molluscan shell proteins. *Comptes Rendus Palevol*, 3(6-7):469–492, October 2004.
[15] Nakahara H, Bevelander G. The formation and growth of the prismatic layer of Pinctada radiata. 7(1):31–45, 1971.
[16] Saleuddin ASM. Shell formation in molluscs with special reference to periostracum formation and shell regeneration. *Pathways in Malacology*, pages 47–81, 1979.
[17] Saleuddin ASM, Petit HP. The mode of formation and the structure of the periostracum. *The Mollusca*, 4(1):199–231, 1983.
[18] Watabe N. Shell. In: Breiter-Hahn, J., Mtoltsky, A.g., Richards, K.S. (eds.): Biology of the integrument. 1, invertebrates. New York: Springer-Verlag; 1984. p 448-485
[19] Checa AG. A new model for periostracum and shell formation in Unionidae (Bivalvia, Mollusca). *Tissue and Cell*, 32(5):405–416, October 2000.
[20] Salas C, Marina P, Checa AG, Rueda JL. The periostracum of Digitaria digitaria (Bivalvia: Astartidae): formation and structure. *Journal of Molluscan Studies*, 78(1):34–43, February 2012.
[21] Dunachie JF. The Periostracum of Mytilus edulis. *Earth and Environmental Science Transactions of the Royal Society of Edinburgh*, 65:383–411, July 1963.
[22] Bubel A. An electron-microscope study of periostracum repair in Mytilus edulis. *Marine Biology*, 20(3):235–244, 1973.
[23] Yonge CM. Mantle fusion in the Lamellibranchia. *Pubbl. staz. zool. Napoli*, 29:151–171, 1957.
[24] Kniprath E. The functional morphology of the embryonic shell-gland in the conchiferous molluscs. *Malacologia*, 18:549–552, 1979. Kniprath1979.
[25] Kessel E. Über den feineren Bau des Mytiliden-Periostracum, erschlossen aus Der Optik. *Zeitschrift für Morphologie und Ökologie der Tiere*, 36(4):581–594, 1940.
[26] Kessel E. Über Periostracum-Bildung. *Zeitschrift für Morphologie und Ökologie der Tiere*, 40(1-3):348–360, 1943.
[27] Waite JH, Andersen SO. 3,4-Dihydroxyphenylalanine (DOPA) and Sclerotization of Periostracum in Mytilus edulis L. *Biological Bulletin*, 158(1):164–173, February 1980.
[28] Tian X, Han Z, Li X, Pu Z, Ren L. Biological coupling anti-wear properties of three typical molluscan shells: Scapharca subcrenata, Rapana venosa and Acanthochiton rubrolineatus. *Science China Technological Sciences*, 53(11):2905–2913, October 2010.
[29] Jia X, Ling X, Tang D. Microstructures and friction-wear characteristics of bivalve shells. *Tribology International*, 39(7):657–662, July 2006.
[30] Tong J, Wang H, Ma Y, Ren L. Two-Body Abrasive Wear of the Outside Shell Surfaces of Mollusc Lamprotula fibrosa Heude, Rapana venosa Valenciennes and Dosinia anus Philippi. *Tribology Letters*, 19(4):331–338, August 2005.
[31] Scherge M, Ahmed SI, Mollenhauer O, Spiller F. Detection of Micronewton Forces in Tribology. *tm - Technisches Messen*, 67(7-8):324-327, July 2000.

[32] Scherge M, Gorb SN. Microtribology of biological materials. *Tribology Letters*, 8(1):1–7, January 2000.
[33] Wählisch FC, Hoth J, Held C, Seyller T, Bennewitz R. Friction and atomic-layer-scale wear of graphitic lubricants on SiC(0001) in dry sliding. *Wear*, 300(1-2):78–81, March 2013.
[34] Oliver WC, Pharr GM. Measurement of hardness and elastic modulus by instrumented indentation: Advances in understanding and refinements to methodology. *Journal of Materials Research*, 19(01):3–20, 2004.
[35] Uskokovic PS, Tang CY, Tsui CP, Ignjatovic N, Uskokovic DP. Micromechanical properties of a hydroxyapatite/poly-l-lactide biocomposite using nanoindentation and modulus mapping. *Journal of the European Ceramic Society*, 27(2-3):1559–1564, January 2007.
[36] Moshe-Drezner H, Shilo D, Dorogoy A, Zolotoyabko E. Nanometer-Scale Mapping of Elastic Modules in Biogenic Composites: The Nacre of Mollusk Shells. *Advanced Functional Materials*, 20(16):2723–2728, August 2010.
[37] Oyen ML. Spherical Indentation Creep Following Ramp Loading. *Journal of Materials Research*, 20:2094–2100, July 2005.
[38] Oyen ML. Analytical techniques for indentation of viscoelastic materials. *Philosophical Magazine*, 86(33-35):5625–5641, November 2006.
[39] Blum MM, Ovaert TC. Experimental and numerical tribological studies of a boundary lubricant functionalized poro-viscoelastic PVA hydrogel in normal contact and sliding. *Journal of the Mechanical Behavior of Biomedical Materials*, 14:248–258, October 2012.
[40] Shipway PH. A mechanical model for particle motion in the micro-scale abrasion wear test. *Wear*, 257(9-10):984–991, November 2004.

Supplementary Figures

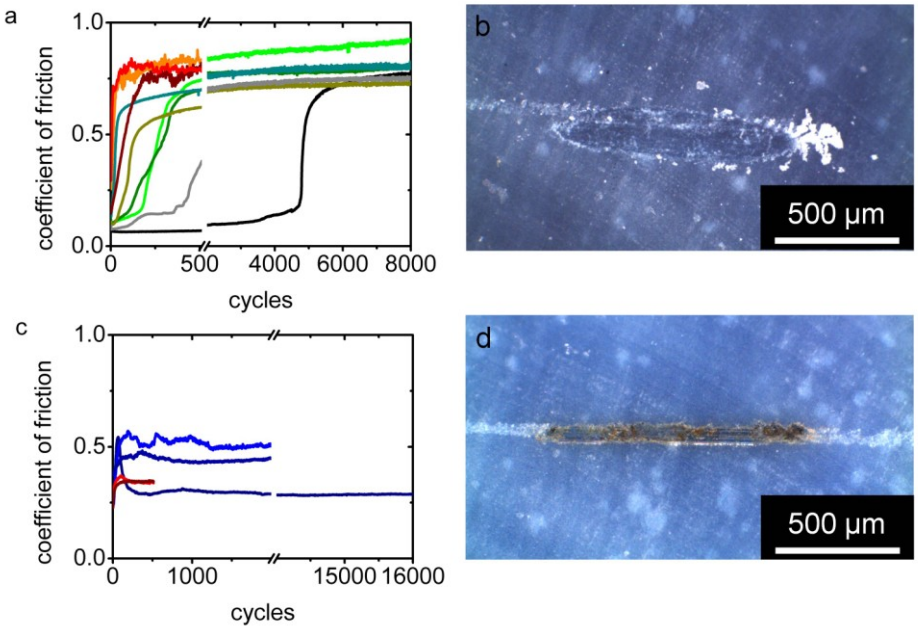

S1: *Long term measurements in dry (a) and wet (c) state, compared with the coefficient of friction determined on the bare calcite fibers. The red lines in (a) and (c) correspond to measurements on the calcite fibers. Figures (b) and (d) show the corresponding wear tracks of the measurements on calcite fibers in dry and wet conditions. The brown colored portions in Figure S1d denote rust from the tribo-chemical wear of the counter body in wet condition.*

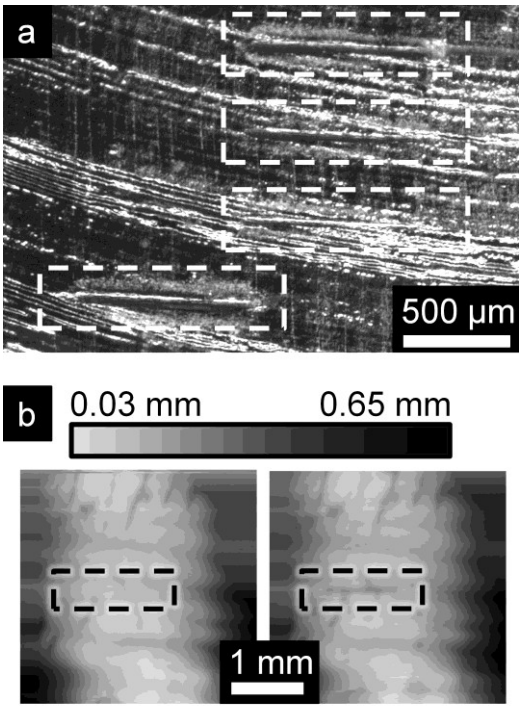

S2: *Images of exemplary wear tracks obtained from long term experiments in dry (a) and in wet state (b). Figure S2a is an optical image, while Figure S2b is a profilometric measurement showing on the left the initial surface of the sample (undamaged and without any wear tracks). The box in the right image in Figure S2b shows the worn surface and wear scar after the long term friction measurement with 16000 cycles in wet condition.*

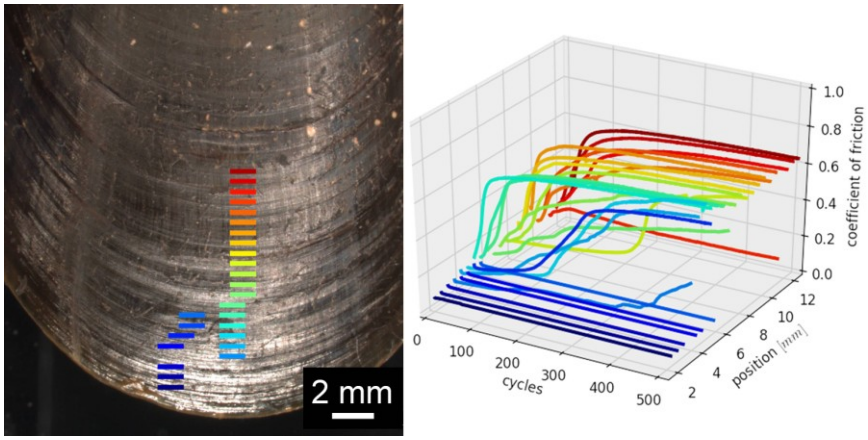

S3: *Measurement areas on a shell and corresponding measurement data. The measurement areas on a shell in dry condition are depicted on the left side. They are selected by the curvature of the area, which must not be too high. The color coded lines correspond to the waterfall plot of the coefficient of friction versus cycle and local offset in one direction on the sample. As can be seen here, the coefficient of friction is usually low on the young parts and increases as the shell parts get older.*

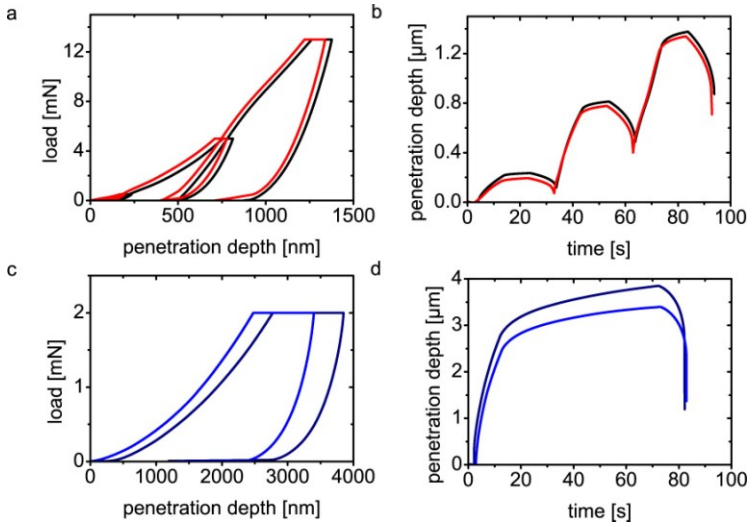

S4: *Selected indentation curves of the load controlled experiments on the periostracum in dry (a), (b) and wet (c), (d) states. While Figure S4a and c show the typical graph of load versus penetration depth, the latter graphs (b), (d) plot the penetration depth versus the time in order to highlight the viscoelastic behavior of the periostracum.*